Available online at www.sciencedirect.com
ScienceDirect
Journal of Solid State Chemistry 180 (2007) 2004–2012
JOURNAL OF SOLID STATE CHEMISTRY
www.elsevier.com/locate/jssc

Synthesis, structure and characterisation of $Fe_{0.50}Ti_2(PO_4)_3$: A new material with Nasicon-like structure

S. Benmokhtar[a,*], A. El Jazouli[a], A. Aatiq[a], J.P. Chaminade[b], P. Gravereau[b], A. Wattiaux[b], L. Fournès[b], J.C. Grenier[b]

[a]*LCMS, UFR Sciences des Matériaux Solides, Faculté des Sciences Ben M'Sik, Casablanca, Morocco*
[b]*Institut de chimie de la matière condensée de Bordeaux (ICMCB-CNRS UPR 9048), Université de Bordeaux1, 33608 Pessac, France*

Received 4 February 2007; received in revised form 23 April 2007; accepted 25 April 2007
Available online 5 May 2007

Abstract

A new iron titanyl phosphate $Fe_{0.50}Ti_2(PO_4)_3$ was synthesized by both solid-state reaction and Cu^{2+}–Fe^{2+} ion exchange method. The material was then characterized by X-ray diffraction, Mössbauer, magnetic susceptibility measurements and optical absorption. The crystal structure of the compound was refined, using X-ray powder diffraction data, by the Rietveld profile method; it crystallizes in the rhombohedral system, space group $R\bar{3}$, with $a = 8.511(1)$ Å and $c = 20.985(3)$ Å, $V = 1316.45(3)$ Å^3 and $Z = 6$. The structure, which is compared to that of $Mn_{0.50}Ti_2(PO_4)_3$ is built up from [TiO_6] octahedra and [PO_4] tetrahedra which are linked by corner sharing along the *c*-axis. Fe^{2+} cations are located in half of the antiprism M_I sites and are orderly distributed with vacancies within the two possible positions of the M_I sites of $R\bar{3}$. These results were supported by the Mössbauer studies that showed the presence of one Fe^{2+} site in the high spin state ($t_{2g}^4 e_g^2$). The Curie–Weiss-type behavior is observed in the magnetic susceptibility. Diffuse reflectance spectrum indicates the presence of octahedrally coordinated Fe^{2+} ions.

Keywords: Synthesis; Phosphate; Nasicon; X-ray diffraction; Mössbauer spectroscopy; Magnetic measurements; UV–visible

1. Introduction

Nasicon-type compounds (acronym for Na superionic conductor) of general stoichiometry $M_xA_2(PO_4)_3$ have been investigated since the early work on $NaZr_2(PO_4)_3$ [1]. This class of compounds exhibits many interesting physical properties such as fast ionic conductivity [2–7], low thermal expansion ceramics [8–11], solid electrolyte, electrode material [12], luminescence [13], high-temperature stability and known for potential as hosts for radioactive waste [14]. Due to these properties they are widely used in high-temperature fuel cells, as catalyst supports, heat exchangers and mirror blanks for space technology [15,16]. The crystal structure of Nasicon-type materials consist of a $[A_2^n(PO_4)_3]^{2n-9}$ framework built up by corner-sharing [AO_6] octahedra and [PO_4] tetrahedra. The basic unit of the framework consists of two [AO_6] octahedra and three [PO_4] tetrahedra which are linked along the *c*-axis. Such ribbons $O_3AO_3MO_3AO_3$ along the *c*-axis are interconnected by [PO_4] tetrahedral units along the *a*-axis. The articulation of these ribbons and chains creates structural holes or interstitial sites in the structure, which can accommodate a variety of *M* ions. There are four such sites per formula unit, as represented by the crystallographic formula $(M_I)(M_{II})_3A_2(PO_4)_3$. The M_I and M_{II} sites have different crystallographic orientations. The M_I sites (type I, one per formula unit) are situated between two [AO_6] octahedra along the *c*-axis with distorted octahedral coordination, while the M_{II} sites (type II, three per formula unit) are larger, with 8–10 coordinating oxygen ions, and are located between the ribbons as shown in Fig. 1. The structure is highly flexible and amenable to substitution on the *M*, *A* or phosphorus sites to form a wide variety of isostructural materials.

The type I and type II site occupancies in the channels may also be varied to form phases in which the number of

*Corresponding author. Fax: +212 22704675.
E-mail address: s.benmokhtar@univh2m.ac.ma (S. Benmokhtar).

0022-4596/$ - see front matter © 2007 Elsevier Inc. All rights reserved.
doi:10.1016/j.jssc.2007.04.014

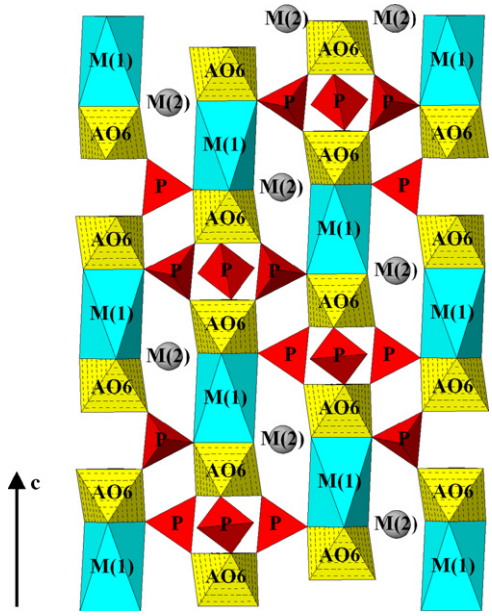

Fig. 1. General view of the rhombohedral $[M_I][M_{II}]_3A_2(PO_4)_3$ Nasicon-type structure.

M ions per formula lies between four (full channels) and zero (empty channels). For example, the compound $Na_5Ti(PO_4)_3$ (crystallographic formula $(Na)_I(Na_3)_{II}NaTi(PO_4)_3$), has sodium ions in both type I and type II sites (0% vacancy) [17]. The compound $NbTi(PO_4)_3$ (crystallographic formula $(\square)_I(\square_3)_{II}NbTi(PO_4)_3$), which has similar framework structure but with completely empty channels (100% vacancy), is capable of incorporating several large ions of electropositive elements [18]. In the compound $Mn_{0.5}Ti_2(PO_4)_3$ (crystallographic formula $(Mn_{0.5})_I(\square_3)_{II}Ti_2(PO_4)_3$) type II sites are empty and type I are partially occupied (50% vacancy) [19]. In the Nasicon family, most of the monovalent cation analogues $M^ITi_2(PO_4)_3$ ($M^+ = Na^+$, Li^+, K^+) [20,21] crystallizes with $R\bar{3}c$ space group. However, the divalent $M^{II}_{0.50}Ti_2(PO_4)_3$ ($M^{2+} = Ca^{2+}$, Sr^{2+}, Mg^{2+}, Co^{2+}, Mn^{2+}, Cu^{2+}) [19,22–26] and trivalent cation $M^{III}_{0.33}Ti_2(PO_4)_3$ ($M^{3+} = La^{3+}$) [27] compounds show extra low-angle reflections, which do not fit into the $R\bar{3}c$ (No. 167) space group. In previous work Barth et al. and Koji Makino et al. [22,28] proposed $R\bar{3}c$ (No. 167) as the space group for magnesium titanium phosphate $Mg_{0.50}Ti_2(PO_4)_3$. El Bouari et al. [23] reported also that $Co_{0.50}Ti_2(PO_4)_3$ crystallizes in a rhombohedral system with $R\bar{3}c$ (No. 167), but recently Olazcuaga et al. [24] studied deeply $Co_{0.50}Ti_2(PO_4)_3$ using the optical and magnetic properties of the polycrystalline $Co_{0.5}Ti_2(PO_4)_3$ which were simultaneously reproduced by use of a crystal field (CF) theory. It turns out that the CF parameters calculated from the structure are in fair agreement with the experimental ones and permit to assign $R32$ (No. 155) as the space group of the crystal structure. Moreover, Fakrane et al. [19] proposed $R\bar{3}$ (No. 148) as the space group for manganese titanium phosphate $Mn_{0.50}Ti_2(PO_4)_3$ isotypic with that of $Ca_{0.50}Ti_2(PO_4)_3$ [25].

In continuation with these types of materials, an attempt is made to synthesize new compounds of the general formula $M_{0.50}Ti_2(PO_4)_3$ (M = Fe, Ni) and insert hydrogen in the channels. In this paper we report only on the preparation of $Fe_{0.50}Ti_2(PO_4)_3$, and its characterization by powder X-ray data, Mössbauer spectroscopy, magnetic susceptibility and UV–visible.

2. Experimental

2.1. Synthesis

The synthesis of $Fe_{0.50}Ti_2(PO_4)_3$ was attempted with two different sets of starting materials. The reactants were weighed separately and ground together in an agate mortar, then the mixture was transferred into a quartz tube and sealed under vacuum, weighed again and put into a furnace for heating treatments.

(i) In the first method, for comparison purposes, the compound was synthesized by heating powders of Fe_2O_3, Fe, TiO_2 with TiP_2O_7 at 600 °C for 6 h and then at 900 °C for 3 days. The reaction was as follows:

$$1/3Fe_2O_3 + 1/3Fe + 3TiP_2O_7 + TiO_2 \rightarrow 2Fe_{0.50}Ti_2(PO_4)_3.$$

(ii) The second method, the $Fe_{0.50}Ti_2(PO_4)_3$ phase was obtained by ion exchange in two stages.

2.1.1. First stage: preparation of $Cu_{0.50}TiO(PO_4)$

The preparation procedure was based on the same method as given in Ref. [29]. Stoichiometric amounts of solutions $Cu(NO_3)_2 \cdot 3H_2O$ (I), $(NH_4)H_2PO_4$ (II) and diluted $TiCl_4$ in ethanol (III) were taken as starting materials. The mixture (precipitate + solution), obtained by slow addition of (III) in (I + II) at room temperature, was dried at about 60 °C to remove the volatile compounds. The resultant powder was sequentially heated at 200 °C (4 h), 750 °C (4 h) and 950 °C (6 h) in oxygen atmosphere with intermediate regrinding. This process resulted in a blue compound $Cu_{0.5}TiO(PO_4)$.

2.1.2. Second stage: preparation of $Fe_{0.50}Ti_2(PO_4)_3$

Amounts of metallic iron, titanyl pyrophosphate and copper titanium oxyphosphate were thoroughly homogenized with the desired composition ratio in an agate mortar. Afterwards, this mixture was sealed in quartz tube under vacuum and dried at 900 °C for 5 days according to the reaction

$$CuTi_2P_2O_{10} + 2TiP_2O_7 + Fe \rightarrow 2Fe_{0.50}Ti_2(PO_4)_3 + Cu.$$

2.2. Instrumental analysis

The X-ray powder diffraction data (XRPD) were collected at room temperature with a Philips PW 3040 (θ–θ) diffractometer using a graphite monochromator.

The structure of the iron phosphate compound was derived from the step-scanned X-ray intensity data, in the range 10–110° (2θ) with a step size of 0.02° (2θ) and counting time of 30 s for each step. The structural parameters were refined by the Rietveld method [30] using the computer program FULLPROF [31].

Mössbauer measurements were performed with a constant acceleration HALDER-type spectrometer using a room-temperature ^{57}Co source [Rh matrix] in the transmission geometry. Isomer shift values refer to α-Fe at 293 K. The spectra were recorded at 4.2 and 293 K using a variable temperature cryostat.

Magnetic susceptibility measurements were carried out with a Quantum Design SQUID MPMS-5S magnetometer. Data were recorded at a constant applied magnetic field ($0 < H < 3$ T) in the temperature range 4.2–340 K.

Optical absorption spectrum has been recorded at room temperature on a Cary 2400 spectrophotometer in the region 210–2400 nm.

3. Results and discussion

In the first and second methods, $Fe_{0.50}Ti_2(PO_4)_3$ was obtained successfully. In the first method, the X-ray powder pattern shows the major phase $Fe_{0.50}Ti_2(PO_4)_3$ together with extra weak lines of Fe_2O_3 (Fig. 2).

The XRPD of the resulting product by the second method show the presence of $Fe_{0.50}Ti_2(PO_4)_3$ and Cu (Fig. 3). Copper was eliminated by leaching with a dilute solution of HNO_3. After filtrating, the sample was washed with distilled water and dried at room temperature. In these conditions a pure iron phase isotype with $Mn_{0.5}Ti_2(PO_4)_3$ [19] is obtained. All the characterizations have been done on the sample obtained by exchange reaction.

The X-ray powder diffraction pattern of the sample obtained in the second experiment is given in Fig. 4 together with that of $Mn_{0.50}Ti_2(PO_4)_3$.

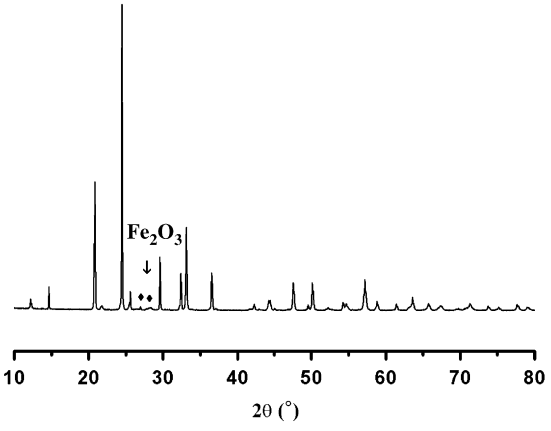

Fig. 2. X-ray powder patterns at room temperature of $Fe_{0.50}Ti_2(PO_4)_3$ prepared by solid-state method.

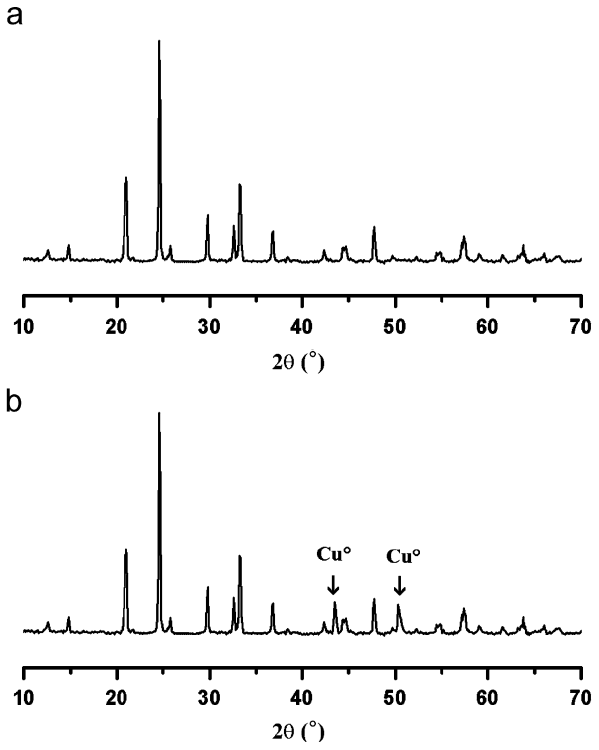

Fig. 3. X-ray powder patterns at room temperature of $Fe_{0.50}Ti_2(PO_4)_3$ prepared by exchange reaction at 900 °C, before (a) and after (b) leaching.

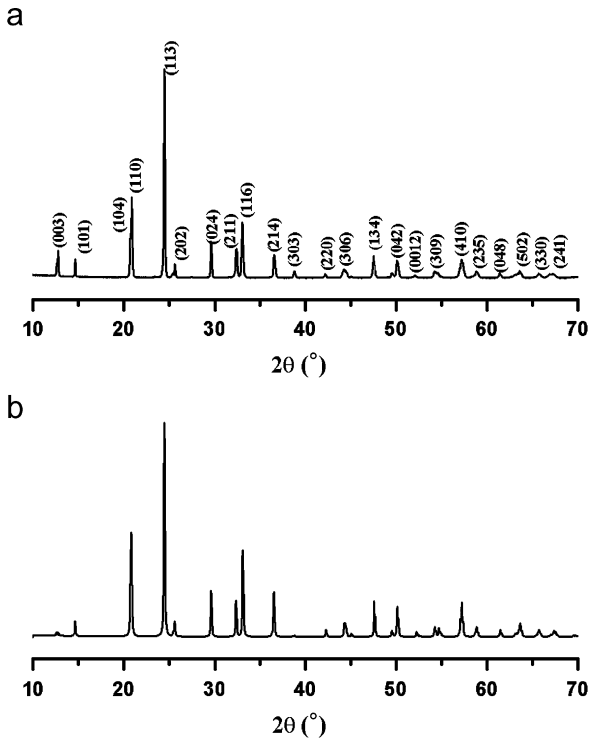

Fig. 4. Powder X-ray diffractograms of $Fe_{0.50}Ti_2(PO_4)_3$ (a) and $Mn_{0.50}Ti_2(PO_4)_3$ (b) [19].

4. Resolution of the structure

The XRPD of $Fe_{0.50}Ti_2(PO_4)_3$ was indexed in the rhombohedral Nasicon type with the cell parameters

Table 1
Comparison of the cell parameters of the Nasicon-type phosphates

$M_{0.50}Ti_2(PO_4)_3$	Space group	$r_M{}^{2+}$ (Å)	a_h (Å)	c_h (Å)	V_h (Å^3)	Ref.
$Mg_{0.50}Ti_2(PO_4)_3$	$R\bar{3}c$	0.72	8.490	20.980	1309	[22]
$Co_{0.50}Ti_2(PO_4)_3$	$R\bar{3}c$, $R32$	0.74	8.510	21.033	1319	[23,24]
$Fe_{0.50}Ti_2(PO_4)_3$	$R\bar{3}$	0.77	8.511	20.985	1316	This work
$Mn_{0.50}Ti_2(PO_4)_3$	$R\bar{3}$	0.83	8.510	21.087	1322	[19]
$Ca_{0.50}Ti_2(PO_4)_3$	$R\bar{3}$	1.00	8.376	22.026	1338	[25]
$Sr_{0.50}Ti_2(PO_4)_3$	$R\bar{3}$	1.16	8.311	22.667	1356	[25]
$Cu_{0.50}Ti_2(PO_4)_3$	$R\bar{3}$	0.73	8.46	21.88	1356	[26]

$a = 8.511(1)$ Å and $c = 20.985(3)$ Å which were comparable to those reported in the literature for similar phases [19,22–26]. The similarities in the cell parameters of $Fe_{0.50}Ti_2(PO_4)_3$ and $M^{II}_{0.50}Ti_2(PO_4)_3$ ($M = Ca^{2+}$, Sr^{2+}, Mg^{2+}, Co^{2+}, Mn^{2+}, Cu^{2+}) (Table 1) suggest that the compounds are isostructural; however, a difference can be noted in space group. XRPD patterns of the compound show the presence of diffraction peaks, with Miller indexes $h\,0\,l$ and $0\,0\,l$ ($l = 2n+1$) [e.g., (101) and (003) reflections], which are not compatible with the presence of the plane c. Therefore the XRPD data could not be indexed completely on the basis of the $R\bar{3}c$ space group but they are consistent with $R32$ and $R\bar{3}$ space groups. As will be shown in the following, by refining the observed intensities of the XRPD data in $R\bar{3}$ and $R32$ space groups, the best agreement was obtained from the $R\bar{3}$ space group.

4.1. Rietveld refinement

The crystal structure of $Fe_{0.50}Ti_2(PO_4)_3$ was refined by the Rietveld method [30], using the FULLPROF program [31]. The refinement was undertaken in two principle models. In the first model it was made in the $R32$ (No. 155) space group whereas in the second the hypothesis of the $R\bar{3}$ (No. 148) space group was verified. In the two models the histogram or phase fraction scale factors, background coefficients, sample displacement error, unit cell parameters, and Lorentzian components of the pseudo-Voigt coefficients adjusted for strain broadening and peak asymmetry were refined first (pattern matching). The results show good agreements in the two space groups. The atomic positions were then refined. The isotropic thermal parameters of all the atoms were then refined freely.

In the first step, the $R32$ crystal structure of $Na_5Ti(PO_4)_3$ [$(Na)_I(Na_3)_{II}TiNa(PO_4)_3$) crystallographic formula] [17] was used as the starting model for the Rietveld refinement. Fe^{2+} and vacancies are randomly distributed in the M_I site, 6c position (001/4), while Ti^{4+} cations are supposed to reside within the framework. The refinement in this model was confirmed to be less appropriate. The results of the refinement in $R32$ shows that the P–O distances were between 1.53 and 1.63 Å, these last values are unrealistic for [PO_4] units. In addition, we should also note that the occupancy factor obtained for Fe^{2+} was negative and its isotropic thermal displacement gives unreasonable value. Thus the refinement in this model seems to be less appropriate. We decided then to refine in $R\bar{3}$.

In the second step, the structural parameters of $Mn_{0.50}Ti_2(PO_4)_3$ [$(Mn_{0.50})_I(\square_3)_{II}Ti_2(PO_4)_3$) crystallographic formula] [19] in the $R\bar{3}$ space group were used as starting parameters for the Rietveld refinement of $Fe_{0.50}Ti_2(PO_4)_3$. Structural refinement of $Fe_{0.50}Ti_2(PO_4)_3$ was realized in two principal steps. In the first step, Fe^{2+} ions

Table 2
Structural data and X-ray Rietveld refinement parameters of $Fe_{0.50}Ti_2(PO_4)_3$

Space group	$R\bar{3}$
a (Å)	8.511(1)
c (Å)	20.985(3)
Volume (Å^3)	1316.45(3)
Wavelength (Å)	$\lambda K_{\alpha1} = 1.54060$; $\lambda K_{\alpha2} = 1.54442$
Step scan increment (2θ)	0.02
2θ range (deg)	10–110
Program	FULLPROF
Zero point (2θ)	0.0170
Pseudo-Voigt function [PV = $\eta L + (1-\eta)G$]	$\eta = 0.504(13)$
Caglioti law parameters	$U = 0.1916(7)$ $V = -0.1567(9)$ $W = 0.0401(2)$
No. of reflections	763
No. of refined parameters	36
R_F	0.076
R_B	0.132
R_P	0.192
R_{wp}	0.233
cR_P[a]	0.224
cR_{wp}[a]	0.291
χ^2	3.02

[a]Without background.

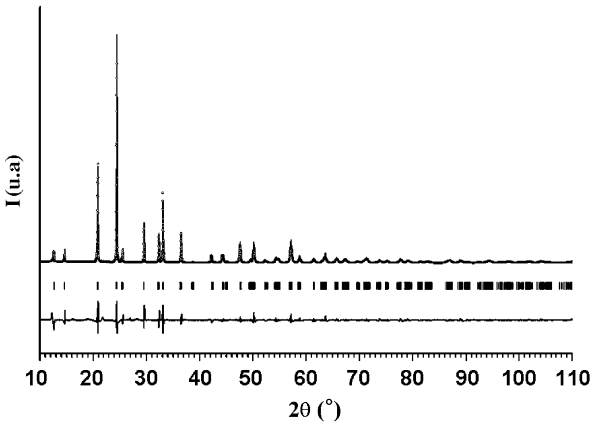

Fig. 5. Final observed (∘∘∘∘) calculated (—) and difference X-ray diffraction patterns for $Fe_{0.50}Ti_2(PO_4)_3$.

Table 3
Atomic coordinates and isotropic temperature factors with their estimated standard deviation corrected with "Berar factor"[32]

Atome	Site	x	y	z	B_{iso} (Å^2)	Occ
Fe(1)	3*a*	0.0	0.0	0.0	1.00(2)	0.73(1)
Fe(2)	3*b*	0.0	0.0	0.50	1.00(2)	0.27 (1)
Ti(1)	6*c*	0.0	0.0	0.1401(12)	0.36(2)	1
Ti(2)	6*c*	0.0	0.0	0.6439(2)	1.61(3)	1
P	18*f*	0.2895(4)	0.0037(7)	0.2486(2)	1.06(1)	1
O(1)	18*f*	0.1817(8)	0.1615(6)	0.0771(1)	1.37(1)	1
O(2)	18*f*	0.1625(7)	0.2003(7)	0.4072(1)	1.37(1)	1
O(3)	18*f*	0.1933(6)	0.9930(9)	0.1869(2)	1.37(1)	1
O(4)	18*f*	0.9723(9)	0.1632(7)	0.3082(2)	1.37(1)	1

are supposed to reside only in one of the two possible types of M_I sites 3*a*, the 3*b* sites were considered to be empty. After several cycles of least-squares refinements, it was shown that the oxygen atoms in 18*f* sites had Biso $= -0.20$ Å^2.

In the second step of refinements, the Fe^{2+} atoms were allowed to occupy the two possible positions of M_I sites (3*a* and 3*b*) instead of only 3*a* in the previous refinement. The total iron content was constrained to 0.50. In this refinement 27% of Fe^{2+} ions are found in the 3*b* position of the M_I site. The final reliability factors for $Fe_{0.50}Ti_2(PO_4)_3$ obtained in the last refinement are $R_P = 0.192$; $R_{WP} = 0.233$; $R_F = 0.076$; $R_B = 0.132$, $\chi^2 = 3.02$. As will be shown in Section 4.3, the relatively high R_B factor value may be related to the presence of a small amount of Fe_2O_3

Table 4
Interatomic distances (Å) and angles (deg) in $Fe_{0.50}Ti_2(PO_4)_3$[a] with their estimated standard deviation corrected with "Berar factor"[32]

$Ti(1)O_6$	O(1)	O(1)	O(1)	O(3)	O(3)	O(3)
O(1)	**1.98(1)**	80.12(78)	80.12(73)	93.33(69)	88.81(68)	167.94(76)
O(1)	2.543(9)	**1.98(1)**	80.12(78)	88.81(39)	167.94(80)	93.33(69)
O(1)	2.543(9)	2.543(7)	**1.98(1)**	167.94(76)	93.33(69)	88.81(69)
O(3)	2.850(7)	2.742(6)	3.896(5)	**1.94(1)**	96.67(71)	96.67(71)
O(3)	2.742(6)	3.896(5)	2.850(7)	2.902(4)	**1.94(1)**	96.67(70)
O(3)	3.896(6)	2.850(7)	2.742(6)	2.902(4)	2.902(4)	**1.94(1)**
$Ti(2)O_6$	O(2)	O(2)	O(2)	O(4)	O(4)	O(4)
O(2)	**1.90(5)**	91.30(45)	91.30(40)	86.60(40)	177.73(50)	89.62(40)
O(2)	2.717(9)	**1.90(5)**	91.30(48)	89.62(38)	86.60(38)	177.73(65)
O(2)	2.717(8)	2.717(9)	**1.90(5)**	177.33(55)	89.62(41)	86.60(38)
O(4)	2.554(7)	2.624(6)	3.722(5)	**1.82(6)**	92.51(44)	92.51(60)
O(4)	3.722(5)	2.554(7)	2.625(6)	2.625(6)	**1.82(6)**	92.51(60)
O(4)	2.625(6)	3.722(5)	2.554(7)	2.625(6)	2.625(6)	**1.82(6)**
$Fe(1)O_6$	O(1)	O(1)	O(1)	O(1)	O(1)	O(1)
O(1)	**2.18(4)**	71.16(33)	71.16(25)	108.84(21)	108.84(22)	180.00(32)
O(1)	2.543(9)	**2.18(5)**	71.16(31)	108.84(21)	180.00(39)	108.84(21)
O(1)	2.543(7)	2.543(7)	**2.18(3)**	180.00(29)	108.84(22)	108.84(21)
O(1)	3.555(3)	3.555(4)	4.371(5)	**2.18(4)**	71.16(25)	71.16(25)
O(1)	3.555(4)	4.371(5)	3.555(4)	2.543(7)	**2.18(5)**	71.16(31)
O(1)	4.371(5)	3.555(4)	3.555(3)	2.543(7)	2.543(7)	**2.18(3)**
$Fe(2)O_6$	O(2)	O(2)	O(2)	O(2)	O(2)	O(2)
O(2)	**2.50(3)**	65.81(23)	65.81(12)	114.19(26)	114.19(16)	180.00(21)
O(2)	2.718(9)	**2.50(4)**	65.81(12)	114.19(26)	180.00(21)	114.19(16)
O(2)	2.718(7)	2.717(9)	**2.50(3)**	180.00(21)	114.19(16)	114.19(16)
O(2)	4.201(3)	4.201(4)	4.943(7)	**2.50(3)**	65.81(23)	65.81(12)
O(2)	4.201(3)	4.943(6)	4.201(4)	2.718(9)	**2.50(4)**	65.81(23)
O(2)	4.943(7)	4.201(3)	4.201(3)	2.718(7)	2.718(7)	**2.50(3)**
PO_4	O(1)	O(2)	O(3)	O(4)		
O(1)	**1.57(7)**	109.66(60)	115.94(62)	101.07(65)		
O(2)	2.531(7)	**1.53(7)**	110.50(61)	106.65(66)		
O(3)	2.609(8)	2.496(7)	**1.51(6)**	112.31(53)		
O(4)	2.426(9)	2.488(7)	2.562(6)	**1.57(8)**		

[a]The M–O distances are given in bold. O–O distances are given below the diagonal and O–M–O angles are given above.

as impurity phase. The crystal data and details of refinement are given in Table 2. Fig. 5 shows the agreement between the calculated and observed diffraction profiles for $Fe_{0.50}Ti_2(PO_4)_3$. The atomic positions and important interatomic distances in the structure are given in Tables 3 and 4, respectively.

4.2. Description of the structure

The structure of $Fe_{0.50}Ti_2(PO_4)_3$ consists of a three-dimensional framework of $[PO_4]$ tetrahedra and $[TiO_6]$ octahedra sharing corners. The $[PO_4]$ tetrahedra are regular with a weak dispersion of the O–P–O angles between 101.07(65)° and 115.94(62)°, which is about the ideal value of 109.45°. The $\langle P–O \rangle$ distance = 1.545(7) Å, which is typical of monophosphate, is close to the distances found in $Mn_{0.50}Ti_2(PO_4)_3$ ($\langle P–O \rangle$ = 1.562(6) Å) [19] and $NaTi_2(PO_4)_3$ ($\langle P–O \rangle$ = 1.543(1) Å) [20]. As emphasized before, iron ions occupy one-half of the M_I sites, with 73% and 27% in the 3*a* and 3*b* sites, respectively. More specifically, the $Fe_1–O_1$ distance, 2.18 Å, is mainly the result of the coulombic attraction, whereas the larger $\square(Fe_2)–O_2$ distance, 2.50 Å, reflects the anionic repulsion in a site, which is almost empty. Finally, since the $[TiO_6]$ octahedra share common faces with the M_I sites: a larger M_I site leads to a smaller neighboring Ti–O distances, and vice versa: $Ti_1–O_1$ (1.98 Å) facing Fe(1) is larger than $Ti_2–O_4$ (1.82 Å) facing the vacancy (Fig. 6).

4.3. Mössbauer spectroscopy

The ^{57}Fe Mössabuer spectra of $Fe_{0.50}Ti_2(PO_4)_3$, recorded at 293 and 4.2 K (Fig. 7) show a quadrupolar doublet with narrow lines. A preliminary refinement using Lorentzian profile lines show that the spectra consist of two fine peaks, the doublet is assigned to Fe^{2+} ions. In the fitting procedure, the two peaks in the quadrupole doublet were

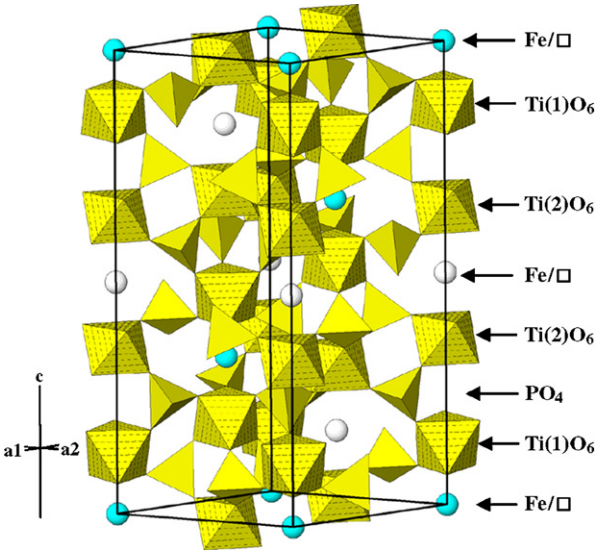

Fig. 6. A polyhedral view of framework as projected in the (*b*, *c*) plane.

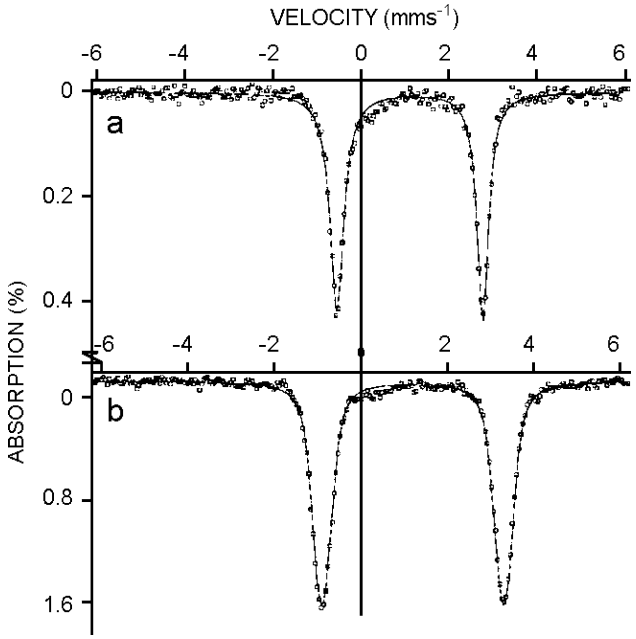

Fig. 7. Mössbauer spectra of $Fe_{0.50}Ti_2(PO_4)_3$ (a) $T = 293$ K, (b) $T = 4.2$ K.

Table 5
Comparison of the Mössbauer parameters of phosphates

Compound	T (K)	δ (mm s^{-1})	Δ (mm s^{-1})	Γ (mm s^{-1})
$Fe_{0.50}Ti_2(PO_4)_3$	293	1.26(1)	3.32(1)	0.38(1)
	4.2	1.36(1)	4.21(1)	0.35(1)
$Fe_3(PO_4)_2$ [33]	295	1.21(2)	2.93(2)	0.28(2)
$(Ni_{0.50}Fe_{0.50})_3(PO_4)_2$ [33]	295	1.21(2)	3.00(2)	0.28(2)
$BaFe_2P_2O_7F_2$ [34]	300	1.22(1)	2.42(1)	0.28(1)
	4.2	1.37(1)	2.56(1)	0.31(1)
$Fe_{0.50}TiO(PO_4)$ [35]	293	1.11(1)	3.85(1)	0.33(1)
	4.2	1.24(1)	4.02(1)	0.30 (1)
$Fe_4O(PO_4)_2$ [36]	300	1.15(1)	2.25(1)	0.26(1)

constrained to have equal intensities and half-widths (Γ). The ^{57}Fe hyperfine parameters for Fe^{2+} found in this study (Table 5) are in good agreement with the ones found previously on the ferrous phosphates compounds [33–36]. The values of isomer shift (δ), quadruple splitting (Δ) and width at half-maximum (Γ) are typical of high-spin Fe^{2+} ions in an octahedral oxygen environment [37,38] with absence of magnetic order at low temperature (4.2 K). These results are in accordance with magnetic results and structural refinements, which indicated the presence of a Fe^{2+} in one site with octahedral environments. Close examination of the both spectra shows a weak impurity line (about 2% of the absorption area) located at about 0.26 mm/s. According to Menil [38], the usual ranges of isomer shifts in iron oxides are 0.29–0.50 and 1.03–1.28 mm/s for Fe(III) and Fe(II) in 6-coordination, respectively; we associate this with the presence of a small

amount of Fe^{3+}, which comes from an impurity phase such as Fe_2O_3 presumably below the limits of detectability by X-ray powder diffraction.

4.4. Magnetic susceptibility

The thermal variation of the reciprocal magnetic susceptibility (Fig. 8) between 4 and 340 K shows a linear behaviour and can be fitted by the simple Curie–Weiss equation: $\chi(T) = C/T - \theta$, where $C = 3.29$ is the Curie constant and $\theta_p = (-3.78 \pm 1)$ K is the Weiss constant. The low negative Weiss constant implies low antiferromagnetic interactions between Fe^{2+} ions, in good agreement with structural data which showed that Fe^{2+} ions are located in isolated oxygen antiprisms with large Fe–Fe distances ($d_{Fe^{2+}-Fe^{2+}} = 6.03$ Å). The experimental effective magnetic moment ($\mu_{eff} = (8C)^{1/2}$) was calculated to be 5.13 μ_B for one Fe^{2+} ion ($3d^6$). This value is typical for the oxidation state (+II) of iron in octahedral sites with high spin configuration (Fe^{2+}: $t_{2g}^4 e_g^2$) [39].

4.5. Optical properties

The optical spectrum of the titanium phosphate $Fe_{0.50}Ti_2(PO_4)_3$ presents two clearly distinct features (Fig. 9): a weak absorption peak in the infrared–visible range and a strong band at the ultraviolet region. This spectrum was successfully deconvolved by three Gaussian bands at lower energy, corresponding to CF electronic absorptions, plus two further bands (one Gaussian and one Lorentzian) at higher energy, probably referable to metal–oxygen charge transfer.

The three CF transitions occur as rather broad bands at ~5115 cm^{-1} (ν_1), ~7610 cm^{-1} (ν_2) and ~11 248 cm^{-1} (ν_3). These transitions can be assigned to Fe^{2+}. The electronic configuration of Fe^{2+} implies a single CF transition $T_{2g}(^5D) \rightarrow E_g(^5D)$ in octahedral coordination, that, however, is often split in three energy levels. On this basis, the transition ν_1 can be attributed to $^5E_g(d_{xz}, d_{yz}) \rightarrow {}^5B_{2g}(d_{xy})$, ν_2 can be assigned to $^5E_g(d_{xz}, d_{yz}) \rightarrow {}^5A_{1g}(^5d_z^2)$, while ν_3 can be assigned to $^5E_g(d_{xz}, d_{yz}) \rightarrow {}^5B_{1g}(d_x^2 - y^2)$ (Fig. 10).

The value of the ligands field parameter (D_q), calculated by fitting the experimental frequencies to an energy-level diagram for octahedral d^6 systems [40], is $D_q = 1034$ cm^{-1}, in good agreement with high spin configuration ($t_{2g}^4 e_g^2$).

The high-energy part of the spectrum is constituted by two intense bands in the near UV (ν_4~21 231 cm^{-1}, ν_5~29 411 cm^{-1}).

The first intense band at ~29 411 cm^{-1} (ν_5) is similar to that of the isostructural phosphate $NaTi_2(PO_4)_3$ (28 546 cm^{-1}) [41], $Mg_{0.50}TiO(PO_4)$ oxyphosphate (27 175 cm^{-1}) [42] and

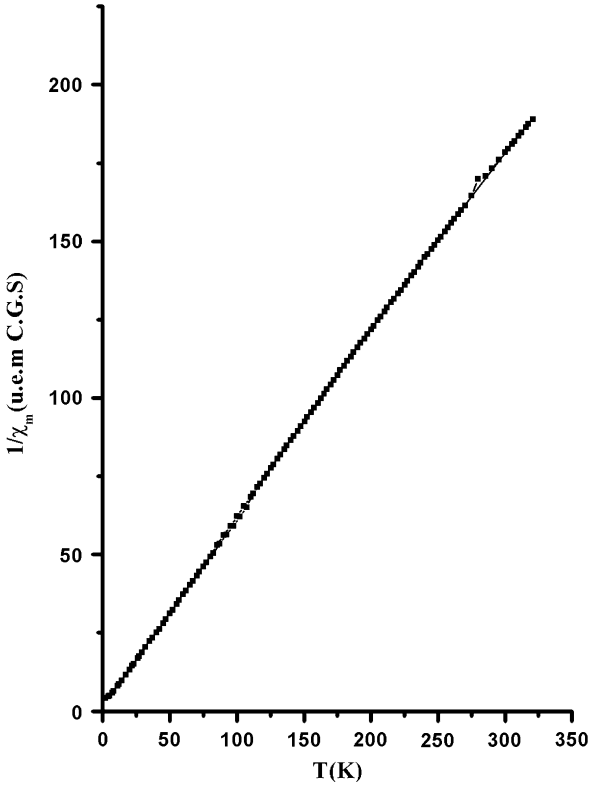

Fig. 8. Reciprocal molar magnetic susceptibility of $Fe_{0.50}Ti_2(PO_4)_3$ as a function of temperature.

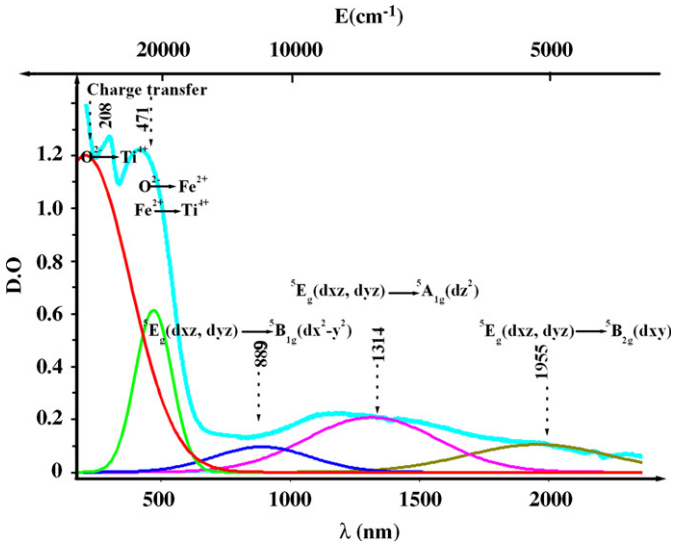

Fig. 9. Diffuse reflectance spectrum of $Fe_{0.50}Ti_2(PO_4)_3$.

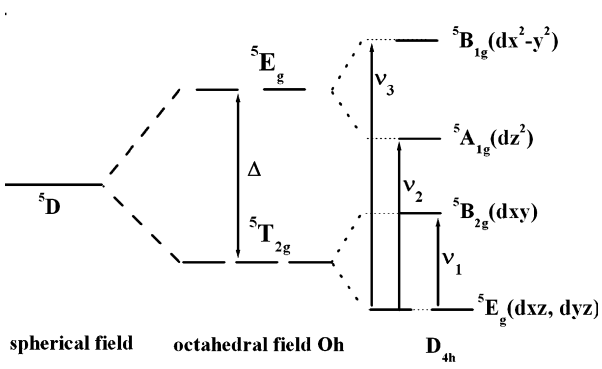

Fig. 10. Schematic energy-level diagram for octahedral Fe^{2+} ion.

also in TiO_2 rutile (24 191 cm^{-1}) [43], this band can be attributed to the electronic charge transfer:

$$O^{2-}(2p^6) + Ti^{4+}(3d^0) \rightarrow O^{-}(2p^5) + Ti^{3+}(3d^1).$$

The evolution of E_g (cm^{-1}) observed for the four crystalline phases is related to the environment of the [TiO_6] octahedron, which is linked to six other [TiO_6] in TiO_2 (rutile), to two [TiO_6] and four [PO_4] in $Mg_{0.50}TiO(PO_4)$ (oxyphosphate) and to six in $Fe_{0.50}Ti_2(PO_4)_3$ or in $NaTi_2(PO_4)_3$ (Nasicon) (Fig. 11). The marked covalence of the P–O bond makes the electronic transfer from oxygen to titanium difficult and explains the high values obtained for the phosphates.

The second intense band at ~21 231 cm^{-1} (v_4) is due to the electronic transfers: $O^{2-} \rightarrow Fe^{2+}$ and $Fe^{2+} \rightarrow Ti^{4+}$ [44].

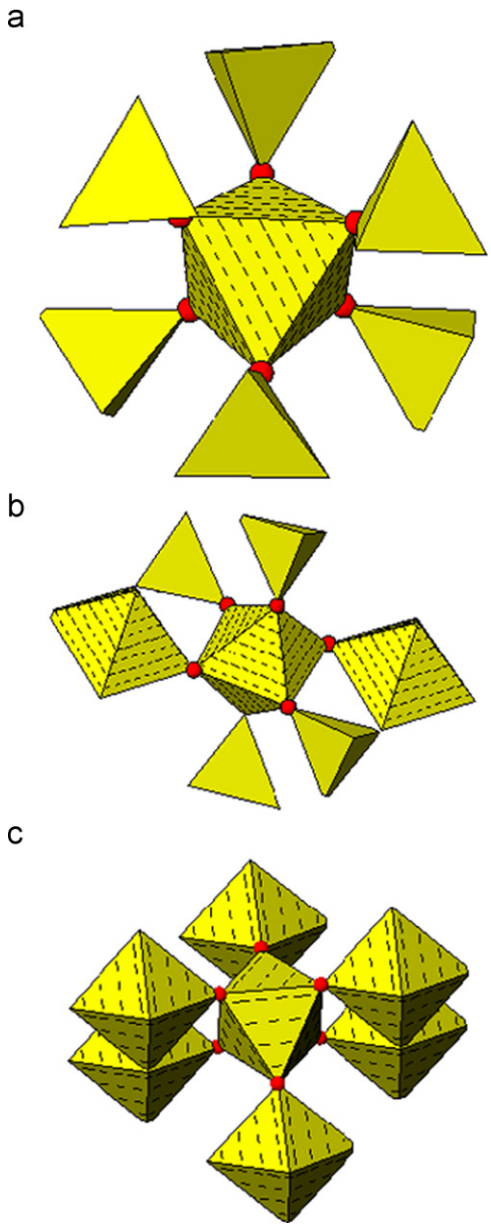

Fig. 11. Titanium environment in $Fe_{0.50}Ti_2(PO_4)_3$ (a), $Mg_{0.50}TiO(PO_4)$ (b), and TiO_2 (c).

5. Conclusion

A new divalent iron-titanium phosphate $Fe_{0.50}Ti_2(PO_4)_3$ has been obtained by two different methods: solid state and ion exchange in quartz sealed tubes. The structure has been refined from X-ray powder diffraction using the Rietveld method. The results revealed that the compound is isotypic with $Mn_{0.50}Ti_2(PO_4)_3$ and belongs to the Nasicon family and crystallizes in the $R\bar{3}$ space group. Fe^{2+} ions occupy partially the M_I sites and are orderly distributed within the two possible positions of the M_I sites [3*a* (000) and 3*b* (001/2)] of $R\bar{3}$. The oxidation state of irons was clearly identified by Mössbauer spectroscopy, magnetic measurement and UV–visible.

Acknowledgments

We wish to thank the ICMCB-CNRS France for support and also E. Lebraud, S. Péchev and O. Viraphong for the technical assistance. Thanks are also due to Dr. B. Manoun for useful discussions.

References

[1] L.O. Hagman, P. Kierkegaard, Acta Chem. Scand. 22 (1968) 1822.
[2] J.B. Goodenough, H.Y.P. Hong, J.A. Kafalas, Mater. Res. Bull. 11 (1976) 203.
[3] Ph. Colomban, Solid State Ionics 21 (1986) 97.
[4] J. Alamo, R. Roy, J. Mater. Sci. 21 (1986) 444.
[5] A. El Jazouli, C. Parent, J.M. Dance, G. Le Flem, P. Hagenmuller, J.C. Viala, J. Solid State Chem. 74 (1988) 377.
[6] K. Arbi, S. Mandal, J.M. Rojo, J. Sanz, Chem. Mater. 14 (2002) 109.
[7] L. Moreno-Real, P. Maldonado-Manso, L. Leon-Reina, E.R. Losilla, F.E. Mouahid, M. Zahir, J. Sanz, J. Mater. Chem. 12 (2002) 3681.
[8] J. Alamo, R. Roy, J. Am. Ceram. Soc. 67 (1984) C78.
[9] R. Roy, D.K. Agrawal, R.A. Roy, Mater. Res. Bull. 19 (1984) 471.
[10] T. Oota, I. Yamai, J. Am. Ceram. Soc. 69 (1986) 1.
[11] S.Y. Limaye, D.K. Agrawal, H.A. Mckinstry, J. Am. Ceram. Soc. 70 (1987) C232.
[12] C. Delmas, F. Cherkaoui, A. Nadiri, P. Hagenmuller, Mater. Res. Bull. 22 (1987) 631.
[13] P. Boutinaud, C. Parent, G. Le Flem, C. Pédrini, B. Moine, J. Phys. Condens. Mater. 4 (1992) 3031.
[14] R. Roy, E.R. Vance, J. Alamo, Mater. Res. Bull. 17 (1982) 3031.
[15] Y. Sheng, H. Sanchio, S. Youichi, M. Norrio, F. Hozumi, Y. Nobru, Chem. Lett. 46 (1991) 2069.
[16] Y. Sheng, S. Youichi, M. Norrio, Y. Nobru, Chem. Lett. 47 (1992) 587.
[17] S. Krimi, I. Mansouri, A. El Jazouli, J.P. Chaminade, P. Gravereau, G. Le Flem, J. Solid State Chem. 105 (1993) 561.
[18] R. Masse, A. Durif, J.C. Guitel, I. Tordjman, Bull. Soc. Fr. Mineral. Cristallogr. 95 (1972) 47.
[19] H. Fakrane, A. Aatiq, M. Lamire, A. El Jazouli, C. Delmas, Ann. Chim. Sci. Mat. 23 (1998) 81.
[20] J.L. Rodrigo, P. Carrasco, J. Alamo, Mater. Res. Bull. 24 (1989) 611.
[21] A. Manthiram, J.B. Goodenough, J. Solid State Chem. 71 (1987) 349.
[22] S. Barth, R. Olazcuaga, P. Gravereau, G. Le Flem, P. Hagenmuller, Mater. Lett. 16 (1993) 96.
[23] A. El Bouari, A. El Jazouli, J.M. Dance, G. Le Flem, R. Olazcuaga, Adv. Mater. Res. 72 (1994) 96.

[24] R. Olazcuaga, J.M. Dance, G. Le Flem, J. Derouet, L. Beaury, P. Porcher, A. EL Bouari, A. El Jazouli, J. Solid State Chem. 143 (1999) 224.
[25] S. Senbhagaraman, T.N. Guru Row, A.M. Umarji, J. Mater. Chem. 3 (1993) 309.
[26] A. El Jazouli, J.L. Soubeyroux, J.M. Dance, G. Le Flem, J. Solid State Chem. 65 (1986) 351.
[27] P. Lightfoot, D.A. Woodcock, J.D. Jorgensen, S. Short, Int. J. Inorg. Mater. 1 (1999) 53.
[28] K. Makino, Y. Katayama, T. Miura, T. Kishi, J. Power Sources 99 (2001) 66.
[29] S. Benmokhtar, H. Belmal, A. El Jazouli, J.P. Chaminade, P. Gravereau, S. Péchev, J.C. Grenier, G. Villeneuve, D. deWaal, J. Solid State Chem. 180 (2007) 772.
[30] H.M. Rietveld, Acta Crystallogr. 22 (1967) 151.
[31] J. Rodriguez-Carvajal, Collected Abstract of Powder Diffraction Meeting, Toulouse, France, 1990, p. 127.
[32] J. F Berrar, P. Lelann, J. Appl. Crystallogr. 24 (1) (1991) 1.
[33] T. Ericsso, A.G. Nord, Am. Mineral. 69 (1984) 889.
[34] J.M. Le Meins, J.M. Grenèche, G. Gourb, J. Solid State Chem. 148 (1999) 286.
[35] S. Benmokhtar, A. El Jazouli, J.P. Chaminade, P. Gravereau, A. Wattiaux, L. Fournès, J.C. Grenier, D. deWaal, J. Solid State Chem. 179 (2006) 3709.
[36] C.C. Gleitzer, Eur. J. Solid State Inorg. Chem. 28 (1991) 77.
[37] N.N. Greenwood, T.C. Gibb, Mössbauer Spectroscopy, Chapman & Hall, London, 1971, p. 77.
[38] F. Menil, J. Phys. Chem. Solids 46 (7) (1985) 763.
[39] C. Kittel, Introduction to Solid State Physics, sixth ed., Wiley, New York, 1986, p. 406.
[40] Y. Tanabe, S. Sugano, J. Phys. Soc. Jpn. 9 (1954) 753.
[41] L.O. Hagman, P. Kierkegaard, Acta Chem. Scand. 22 (1968) 1822.
[42] S. Benmokhtar, A. El Jazouli, S. Krimi, J.P. Chaminade, P. Gravereau, M. Menetrier, D. de Waal, Mater. Res. Bull. 42 (2007) 892.
[43] D.E. Scaife, Sol. Energy 25 (1) (1980) 41.
[44] M.G. Clark, F.J. DiSalvo, A.M. Glass, G.E. Peterson, J. Chem. Phys. 59 (1973) 6209.